



Article

# Differential Urinary Proteomic Analysis of High-Risk Cervical Intraepithelial Neoplasia

Peter Bober <sup>1,\*</sup>, Soňa Tkáčiková <sup>1</sup>, Ivan Talian <sup>1</sup>, Peter Urdzík <sup>2</sup>, Silvia Toporcerová <sup>2</sup> and Ján Sabo <sup>1,\*</sup>

<sup>1</sup> Department of Medical and Clinical Biophysics, Faculty of Medicine, University of Pavol Jozef Šafárik in Košice, Trieda SNP 1, 04011 Košice, Slovakia

<sup>2</sup> Department of Gynaecology and Obstetrics, Faculty of Medicine, University of Pavol Jozef Šafárik in Košice, Trieda SNP 1, 04011 Košice, Slovakia

\* Correspondence: peter.bober@upjs.sk (P.B.); jan.sabo@upjs.sk (J.S.)

**Abstract:** Human papillomavirus (HPV)-associated lesions and malignancies exhibit alterations in the composition and functionality of the extracellular matrix (ECM) that represent the complex molecular pathways present between infection and disease. A total of 20 urine samples were used, including from 10 patients with cervical intraepithelial neoplasia grade 3 (CIN3) and 10 healthy controls to perform the label-free quantitative analysis using the nano-HPLC and ESI-MS ion trap mass analyzer and matrix-assisted laser desorption ionization–time-of-flight mass spectrometry (MALDI-TOF/MS) fast screening. Among 476 identified/quantified proteins, 48 were significantly changed ( $\log_2$ -fold change  $\geq 1.0$  or  $\leq -1.0$ ,  $-\log_{10}$  (b)binomial,  $p$ -value  $\geq 1.3$ ), of which were 40 proteins (down-regulated) and 8 proteins (up-regulated) in CIN3, in comparison to healthy controls. The biological function and key pathway enrichment of the gene set using gene set enrichment analysis (GSEA) were analyzed. The ECM-receptor interaction pathway (NES =  $-1.64$ ,  $p = 0.026$ ) was down-regulated by 13 proteins (HSPG2, COL6A1, COL6A3, SPP1, THBS1, TNC, DAG1, FN1, COMP, GP6, VTN, SDC1, and CD44;  $\log_2$  FC range from  $-0.03$  to  $-1.48$ ) for the CIN3 group in the KEGG database. The MALDI-TOF/MS screening showed the difference of protein profiles between the control and CIN3 groups, i.e., using the scatter plot with a well-separated shape, as well as effectively distinguishing both groups (control and CIN3) using genetic algorithms (GA) with cross-validation (51.56%) and recognition capability (95.0%). Decreased levels of ECM-receptor interaction proteins may cause disturbances in the interactions of cells with the ECM and play an important role in the development and progression of cervical cancer.

**Keywords:** urine; cervical intraepithelial neoplasia; extracellular matrix; heparan sulfate proteoglycans; proteomic analysis



**Citation:** Bober, P.; Tkáčiková, S.; Talian, I.; Urdzík, P.; Toporcerová, S.; Sabo, J. Differential Urinary Proteomic Analysis of High-Risk Cervical Intraepithelial Neoplasia. *Int. J. Mol. Sci.* **2023**, *24*, 2531. <https://doi.org/10.3390/ijms24032531>

Academic Editor: Subhasis B. Biswas

Received: 2 December 2022  
Revised: 24 January 2023  
Accepted: 25 January 2023  
Published: 28 January 2023



**Copyright:** © 2023 by the authors. Licensee MDPI, Basel, Switzerland. This article is an open access article distributed under the terms and conditions of the Creative Commons Attribution (CC BY) license (<https://creativecommons.org/licenses/by/4.0/>).

## 1. Introduction

Cervical cancer is most commonly caused by HPV, a tiny, non-enveloped dsDNA virus belonging to the Papillomaviridae family [1]. In terms of cancer-related fatalities among women globally, cervical cancer ranks fourth [2]. More than 90% of high-grade squamous intraepithelial lesions (HSIL or CIN2+) include HPV, which is found in nearly all cervical cancer biopsy samples [3]. Currently, more than 200 different HPV genotypes are known [4]. Of them, HPV 16 and HPV 18 constitute the high-risk oncogenic genotypes, since they are responsible for over 70% of all cervical cancer [5–7].

Cervical intraepithelial neoplasia (CIN) presents a precursor lesion where the cervical cancer development begins. High-grade precancerous lesions (CIN2 and CIN3) may appear 3 to 5 years after persistent, high-risk HPV infections. The precancerous lesion of a more advanced cervical cancer, CIN3 (carcinoma in situ-CIS), is a morphologically heterogeneous disease [8].

The dysregulation of proteins that alter the ECM and abnormalities in cell–ECM interactions are key factors in the initiation and progression of many kinds of cancers [9].

Malignant transformation is thought to be characterized by a changed interaction between the ECM and tumor cells [10]. In HPV-associated lesions and malignancies such as cervical cancer, structural and functional alterations of the ECM are frequent [8].

The effectiveness of urine-based, high-risk human papillomavirus (hrHPV) testing for CIN3 identification is less obvious in contrast to the cytology or histology evaluations of cervicovaginal samples, since studies employ a variety of hrHPV assays and non-standardized urine collection methods [11,12]. Nevertheless, due to its low cost, non-invasive nature, and ease of collection, urine samples may be utilized for women who choose not to undergo regular tests [13,14].

In order to compare the protein expression profiles between the urine of healthy controls and CIN3 patients, label-free quantification using nano-HPLC coupled with ion trap mass analyzer and the MALDI-TOF/MS technique was applied in the present study. Currently, literature on scientific studies clarifying the connection between HPV infection and CIN3 status and comparing the proteomic profiles of CIN3 patients to the healthy controls in urine samples are limited. Consequently, our study may assist in elucidating possible biomarkers of CIN3 from urine samples.

## 2. Results

### 2.1. Urine Proteomic Analysis Using the MALDI-TOF/MS and ESI-MS Ion Trap

The total of 20 urine samples, including 10 patients with CIN3 and 10 healthy controls, were used. The difference in the protein profiles between the control and CIN3 groups obtained by MALDI-TOF/MS fast screening analysis was recorded. Proteomic analysis was carried out using the label-free quantitative approach (spectral count) by nano-HPLC and ESI-MS ion trap mass spectrometer.

### 2.2. MALDI-TOF/MS Detection Model Generation

Classification models were generated using three algorithms (GA, SNN and QC) to distinguish the control group and the CIN3 group in the urine samples. For all these models, to classify mass spectra, the default setting was used. Specifically, for the GA model: maximal number of peaks in the model—10, maximal number of generations—50, number of neighbors—3, initial number of peak combinations—automatic detection, mutation rate—0.2, and crossover rate—0.5; for SNN: upper limit of cycles—10 × 100 and automatic detection of prototype number; and for QC: *p*-value *T*-Test/ANOVA.

Cross-validation (CV) and recognition capability (RC), which represent each model's performance, were employed. In MALDI TOF/MS analysis, the model with the highest RC value was used. The GA model had the highest value of recognition capability (95.0%). In contrast, the model with the highest cross-validation value (62.66%) was the QC model. However, SNN and GA classification models had very comparable cross-validation values, which were 51.02% and 51.56%, respectively (Table 1).

**Table 1.** Results of a cross-validation test and recognition capability test of the GA, SNN, and QC models to distinguish the two groups (control and CIN3) in the urine samples.

Samples	Model	Generated Peaks	Cross-Validation (%)	Recognition Capability (%)
urine	GA	10	51.56	95.00
	SNN	15	51.02	90.00
	QC	3	62.66	85.00

The 10 mass peaks/integration areas with the highest recognition capability were chosen using the GA classification model and are depicted by red bars (*m/z* 2050.8, 2200.6, 2291.0, 2618.7, 3343.6, 3377.6, 3414.6, 6525.5, 15,514.5 and 18,202.8) in the urine samples (from a total of 60 mass peaks indicated by blue bars) (Figure 1). Differences between the control and the CIN3 groups in the expression levels of the total average spectra of several ions (in red and green, respectively) generated by the GA model are depicted in Figure 1A–D as zoomed-in small graphs.

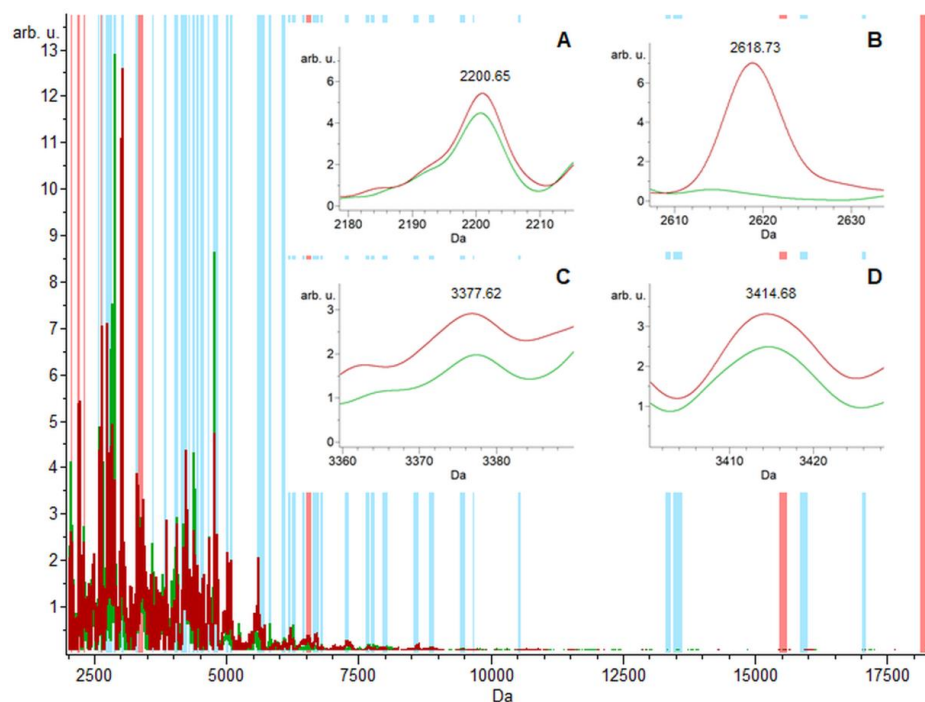


**Figure 1.** The location of discriminating peak masses,  $m/z$  2050.8, 2200.6, 2291.0, 2618.7, 3343.6, 3377.6, 3414.6, 6525.5, 15,514.5, and 18,202.8, determined by the GA model with the highest recognition capability. (A–D) The zoomed-in total average spectra of several ions displaying differential expression levels in the groups; control and CIN3, depicted in red and green, respectively, of the urine samples.

### 2.3. MALDI-TOF/MS Cluster Analysis

The cluster analysis by 2D peak distribution of the peaks at 2618.7 and 3010.0  $m/z$  manifested their discriminating capability between the CIN3 group and the control group in the urine samples (Figure 2A, Table 2).

### 2.4. ESI-MS Analysis and Label-Free Quantitative Comparisons of Differentially Expressed Proteins in the Urine between CIN3 and Healthy Controls

We performed label-free quantitative proteomic analysis to identify potential biomarkers in urine samples. Among the 476 total proteins identified/quantified, 48 proteins were significantly altered ( $\log_2$ -fold change  $\geq 1.0$  or  $\leq -1.0$ ,  $-\log_{10}$  (bbinomial),  $p$ -value  $\geq 1.3$ ), of which there were 40 proteins that were down-regulated and 8 proteins that were up-regulated in the CIN3 group, in comparison to the healthy controls (Table S1 (see Supplementary Materials), Figure 3).

### 2.5. ESI-MS Analysis and Pathway Enrichment Analysis of the Differential Urine Proteins in CIN3 versus Control Samples

The biological function and key pathway enrichment of the gene set between control and CIN3 in the urine samples were analyzed using GSEA in the KEGG database. As a result, the enriched pathway was obtained, namely the ECM-receptor interaction (normalized enrichment score; NES =  $-1.64$ ,  $p = 0.026$ ) shown on Figure 4A. The 16 core enrichment genes of the ECM-receptor interaction are shown in Figure 4B. In this pathway, a remarkably high number of genes were altered, e.g., of the all 88 proteins in the ECM-receptor interaction pathway, 15 showed a regulatory change using the Pathview Web Server (Figure 5). Among them were seven core enrichment proteins, i.e., a subset of genes that contributed most to the enrichment result (HSPG2, COL6A1, COL6A3, SPP1, THBS1, TNC, and DAG1). We found that the ECM-receptor interaction pathway was downregulated by 13 proteins (HSPG2, COL6A1, COL6A3, SPP1, THBS1, TNC, DAG1,

FN1, COMP, GP6, VTN, SDC1, and CD44;  $\log_2$  FC range from  $-0.03$  to  $-1.48$ ) and up regulated by 2 proteins (TNXB and COL4A2;  $\log_2$  FC =  $0.09 - 0.14$ ) for the CIN3 group in the KEGG database. Among them, only HSPG2 was significantly changed ( $\log_2$  FC =  $-1.48$ ,  $p$ -value =  $0.002$ ) (Table S1, Figure 4B).

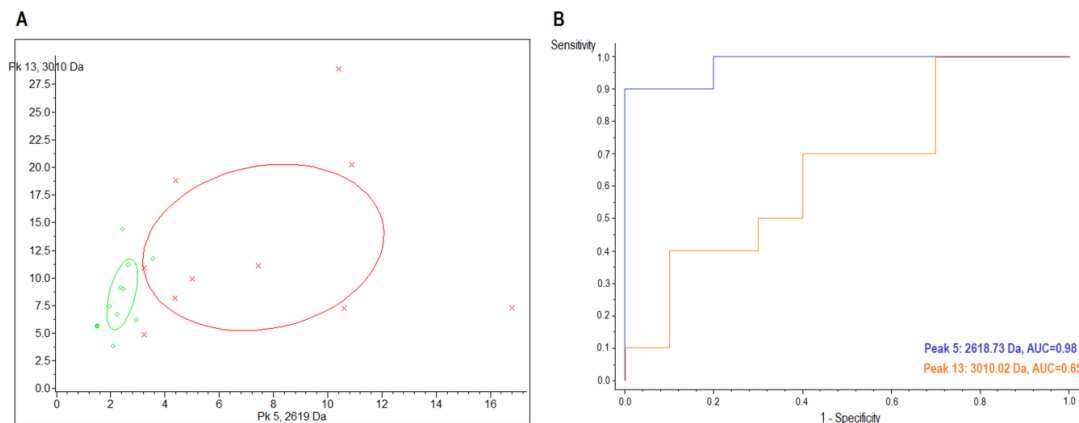


**Figure 2.** (A) Scatter plot of the urine samples determined by the combination of peptide/protein, with  $m/z$  2618.7 (x-axis) and 3010.0 (y-axis) (peaks with lowest  $p$ -values) between healthy control subjects (red) and CIN3 (green) patients. Confidence intervals of 95% are shown by ellipses. (B) ROC curve plots showing the correlation between the sensitivity and specificity of the  $m/z$  2618.7 (blue) and 3010.0 (orange). Areas under the ROC curves (AUC) are 0.98 and 0.65, respectively.

**Table 2.** Statistical analysis of the most discriminating protein or polypeptide ions in the cluster analysis by 2D peak distribution.

Sample	Index Peak	Mass ( $m/z$ )	Dave <sup>1</sup>	PTTA <sup>2</sup>	PWKW <sup>3</sup>	PAD <sup>4</sup>	Control (avg <sup>5</sup> $\pm$ SD <sup>6</sup> )	CIN3 (avg $\pm$ SD)	AUC
urine	5	2618.73	5.79	0.289	0.0026	0.000219	$8.48 \pm 4.94$	$2.69 \pm 0.63$	0.98
	13	3010.02	4.71	0.59	0.672	0.00872	$14.17 \pm 8.36$	$9.46 \pm 3.55$	0.65

<sup>1</sup> Difference between the maximal and minimal average peak area/intensity of all classes. <sup>2</sup>  $p$ -value of  $t$  test. <sup>3</sup>  $p$  value of Wilcoxon test. <sup>4</sup>  $p$ -value of Anderson–Darling test. <sup>5</sup> peak area/intensity average of class. <sup>6</sup> Standard deviation of the peak area/intensity average of class.

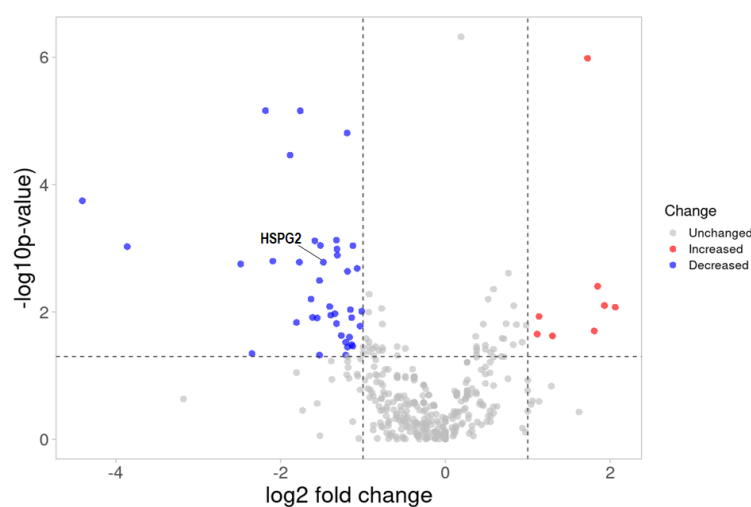


**Figure 3.** Volcano plot of the 476 differentially expressed proteins between the CIN3 and healthy controls. The 48 proteins that were significantly changed ( $p$ -value less than 0.05 and  $\log_2$ -fold change  $\geq 1.0$  or  $\leq -1.0$ ), i.e., 8 up-regulated (red) and 40 down-regulated (blue) proteins. Volcano plots were generated with the VolcanoR online web tool with R/Shiny (<https://huygens.science.uva.nl/VolcanoR>, accessed on 16 November 2022).



### 3. Discussion

Using a wide range of hrHPV DNA tests, several studies examined the hrHPV concordance between urine vs vaginal self-samples and cervical specimens collected by the doctor [15–21]. However, the direct comparison of different hrHPV DNA tests within the same research has received minimal attention [18,21]; hence, no relevant conclusions about their effects exist. MS-based proteomics has recently become a more potent technique for protein quantification, as well as their identification [22]. By comparing protein expressions across different types of samples or treatments, protein quantification can boost the quantity of relevant information [23].

Thanks to MALDI-TOF/MS analysis, the differences in protein profiles between the control and CIN3 groups were confirmed, and both groups (control vs. CIN3) were effectively distinguished. In most cases, the highest mass peak intensity (total average spectra) in the control group, compared to CIN3, were detected using the GA model with the highest sensitivity (95.00%) (Table 1, Figure 1). Moreover, MALDI-TOF/MS showed a potential to be used as a fast and simple screening method for CIN3 identification in urine samples.

Our ESI-MS results of the label-free quantification in the compared groups confirmed the hypothesis of the possibility of classifying the samples (control vs. CIN3) using MALDI-TOF/MS based on their different urine proteomic profiles. The results presented in Table S1 and Figure 5 indicate decreased levels of the 13 proteins (HSPG2, COL6A1, COL6A3, SPP1, THBS1, TNC, DAG1, FN1, COMP, GP6, VTN, SDC1, and CD44) in the ECM-receptor interaction signaling pathway (NES =  $-1.64$ ,  $p = 0.026$ ) (Figure 4). However, only one protein (HSPG2) with significant change ( $\log_2$  FC =  $-1.48$ ,  $p$ -value =  $0.002$ ) was detected (Figure 3). From the ECM-receptor interaction pathway analysis, it can be concluded that a decrease in the levels of ECM proteins may cause disturbances in the interactions of cells with the ECM and plays an important role in the development and progression of cervical cancer.

For healthy growth and tissue homeostasis, interactions between cells and the surrounding matrix, as well as within the ECM, are essential [24]. ECM interactions are complex, generating signals that control key cellular activities such as adhesion, differentiation, motility, autophagy, proliferation, and apoptosis [25–27]. These cellular processes are regulated by the ECM-receptor interaction pathway [28]. The progression of several malignancies, including breast cancer, prostate cancer, and gastric cancer, is contributed by this pathway [29–31]. Wu et al. discovered that the ECM-receptor interaction pathway was the key pathway during CC development using datasets from the GEO database [32]. Moreover, Ramirez-Torres et al. discovered that the ECM-receptor interaction pathway was down-regulated (NES =  $-2.17$ ,  $p < 0.01$ ) in cervical cancer, compared to control [33]. HPV-associated lesions and malignancies exhibit alterations in the ECM's structure and functionality, leading to intricate molecular pathways that link infection with disease [11]. In the last period, the ECM changes in cervical cancer were investigated, including the expressions and activities of galectins, collagens, proteoglycans, laminins, fibronectins, integrins, proteases, and regulators [8].

The HPV infection cycle starts with the initial contact, which is mostly mediated by HSPGs that are expressed on the basal keratinocytes' cellular surface or on the ECM. Thus, HSPG proteins have an important role in the HPV infection in regard to their initial attachment [34,35]. Perlecan (HSPG2), a multidomain protein present in all basement membranes, represents the most significant proteoglycan. Perlecan is a found, natural component of the basal membrane of skeletal muscle and participates in the interaction with  $\alpha$ -dystroglycan [35]. The dystroglycan complex's  $\alpha$ -subunit mediates its interaction with components of ECM [36]. The findings of Sgambato et al. showed that a decrease in the expression and function of the dystroglycan complex was associated with the onset of cervical cancer and that it may be crucial in the early stages of the disease [37]. Additionally, according to Zhang et al., cervical cancer patients had considerably lower levels of HSPG2 expression than healthy individuals [38]. Furthermore, the results of Ramirez-Torres et al. showed the downregulation of collagens (COL6A1 and COL6A3) in cervical cancer, compared to the control [33]. Additionally, it was previously demonstrated that lower

expression of syndecan-1 (SDC1) correlates with enhanced tumorigenicity, i.e., as CIN developed into microinvasive carcinoma, the SDC1 expression level was decreased [39,40]. More than 50% of invasive carcinomas and CIN2+ lesions had decreased CD44 expression, which may be related to loss of cellular adhesion [41]. It has been established that HPV oncogenes inhibited the fibronectin (FN1) promoter [42] and reduced the expression of thrombospondin-1 (THBS1) as potent angiogenesis inhibitors in human keratinocytes [43].

## 4. Materials and Methods

### 4.1. Patient's Selection

Written informed consent was obtained from women in the control group and the biopsy-proven cervical intraepithelial neoplasia (CIN3) group for urine sampling utilized for research purposes (EK/06045/2020). Randomized urine samples were taken from the Department of Gynecology and Obstetrics, Faculty of Medicine, University of Pavol Jozef Šafárik in Košice, in the period from 1 September to 31 December 2020. Of these, 10 control samples were obtained from healthy donors, with a mean age of 36 years (range: 27–46 years), and 10 patients with CIN3, with a mean age of 34 years (range: 30–39 years).

### 4.2. Urine Sampling

Urine (50 mL) was collected in a sterile tube. All samples were cooled at 4 °C and processed within 30 min. Subsequently, urine samples were centrifuged (2500× *g*, 4 °C, 45 min) to remove cell debris. Urine samples, prior to freezing (−80 °C), were supplemented with the Calbiochem EDTA-free Protease Inhibitor Cocktail Set III (Merck Millipore, Burlington, MA, USA), at a dilution of 1/1000–1/2000, and sodium azide (NaN<sub>3</sub>, 0.02% *v/v*).

### 4.3. Sample and Matrix Preparation for MALDI-TOF/MS Analysis

Vortexing was performed on the urine samples that had been defrosted. A Microcon-30 kDa Centrifugal Filter Unit (Merck KGaA, Darmstadt, Germany) was activated with 100 µL of 0.1% TFA, followed by centrifugation at 14,000× *g* for 10 min. Then, 400 µL of human urine samples (diluted 1:5 with TFA 0.5%) were loaded and centrifuged at 14,000× *g* for 30 min. The protein eluate (≤30 kDa) was collected, desalted, and concentrated with a C18 ZipTip® (Millipore, Billerica, MA, USA), as described in the specification sheet. All samples were acidified with concentrated trifluoroacetic acid (TFA) (Sigma-Aldrich, St. Louis, MO, USA) to a pH ≤ 4. After that, 1 µL of the sample was spotted onto a MALDI MTP 384 target plate polished steel (Bruker Daltonics GmbH, Bremen, Germany). One microliter of the matrix solution, which contained α-cyano-4-hydroxycinnamic acid (HCCA) (Sigma Aldrich, St. Louis, MO, USA), diluted in ACN/H<sub>2</sub>O (1:1, *v/v*) with 2.5% TFA, was applied to the air-dried sample. The MALDI-TOF/MS was used to measure the mass spectra of all samples in the positive linear mode (Bruker Daltonics GmbH, Bremen, Germany). Acquisition parameters were used as follows: *m/z* range of 1500–20,000; a matrix suppression cutoff at *m/z* 1000; two 1000-shot laser pulses; and a protein calibration standard (Bruker Daltonics, Bremen, Germany). The ClinProTools software for MALDI-TOF/MS data analysis (version 3.0; Bruker Daltonics GmbH, Bremen, Germany) was employed. Raw data preprocessing included baseline subtraction using the top hat algorithm at minimum the baseline width (10%) and smoothing with 10 cycles of a Savitzky–Golay (S-G) filter with a width of 5 *m/z* and a mass range *m/z* of 2000 to 20,000.

### 4.4. Sample Processing for LC-MS/MS Analysis

A Centriprep® Ultrafiltration Centrifugal Filter (10 kDa MWCO, Merck KGaA, Darmstadt, Germany) was used, activated with 10 mL of redistilled water, then centrifuged (20 °C, 3000× *g*, 30 min). An amount of 10 mL of the urine samples was added, followed by centrifugation. Subsequently, 0.005 M NaCl (10 mL) was added and centrifuged. The previous step was repeated once more. The obtained supernatant (4 mL) was added to an Amicon® Ultra-4 Centrifugal Filter Unit (3 kDa MWCO, Merck KGaA, Darmstadt, Germany) and centrifuged (4 °C, 7000× *g*, 30 min). The concentration of proteins was

determined using the Bradford method with 4  $\mu\text{L}$  of the sample. An amount of 100  $\mu\text{L}$  of 10 mM DTT in 8 M urea (in 100 mM TRIS/HCl, pH 8) was added to the extracted proteins, mixed in a thermomixer (45 min at 37 °C), and centrifuged ( $1000\times g$ , 10 min at 4 °C). Next, 100  $\mu\text{L}$  of 50 mM IAA in 8 M urea (in 100 mM TRIS/HCl, pH 8) was added, thermomixed (30 min at 37 °C in the dark), and centrifuged. The protein solution was washed using ACN/water (1/1, 500  $\mu\text{L}$ ), thermomixed (20 °C, 10 min), and centrifuged ( $2500\times g$ , 10 min, 4 °C). Subsequently, the solution was washed with 0.1 M  $\text{NH}_4\text{HCO}_3$  (500  $\mu\text{L}$ ) and centrifuged ( $3500\times g$  for 10 min at 4 °C). The previous step was repeated once more. The 0.1 M  $\text{NH}_4\text{HCO}_3$  (100  $\mu\text{L}$ ) containing 0.002 M  $\text{CaCl}_2$  and trypsin (35  $\mu\text{L}$ , overnight digestion) was added to the protein solution. Subsequently, the samples were centrifuged ( $7000\times g$ , 55 min, 4 °C). Peptides were acidified with concentrated formic acid (FA) to a  $\text{pH} \leq 4$ .

#### 4.5. LC-MS/MS Analysis and Database Search

The nanoliquid HPLC (Ultimate 3000 RSLC Nano, Thermo Fisher Scientific, Germering, Germany), coupled with an amaZon speed ETD ion trap mass spectrometer (Bruker Daltonik, Bremen, Germany) interfaced with CaptiveSpray ion source (Bruker Daltonik, Bremen, Germany), was used to analyze the urine samples. The Acclaim<sup>®</sup> PepMap 100 C<sub>18</sub> trap column (100  $\mu\text{m} \times 2 \text{ cm}$ , 5  $\mu\text{m}$  particles, 100 Å) was loaded with a 1  $\mu\text{L}$  sample (1  $\mu\text{g}$  of peptides), which included 1  $\mu\text{g}$  of peptides using the mobile phase (98% H<sub>2</sub>O and 2% ACN with 0.1% FA) at an 8  $\mu\text{L min}^{-1}$  flow rate. The following step involved washing the peptide from the trap column to the Acclaim<sup>®</sup> PepMap RSLC C<sub>18</sub> analytical column (75  $\mu\text{m} \times 15 \text{ cm}$ , 3  $\mu\text{m}$  particles, 100 Å) and eluting them to ESI-MS. Gradient elution was as follows: a 96% mobile phase A (98% H<sub>2</sub>O and 2% ACN with 0.1% FA) and 4% mobile phase B (95% ACN and 5% H<sub>2</sub>O with 0.1% FA) ratio was kept for 5 min. The 4% mobile phase B increased to 35% mobile phase B in the next 90 mins of the HPLC run. The 95% mobile phase B was kept from 95 to 105 min for a column wash, followed by column equilibration with 4% mobile phase B for 120 min. A 0.4  $\mu\text{L min}^{-1}$  flow rate was used. MS scan parameters: positive ion mode charges, enhanced resolution scans, ion charge control (ICC) at 400,000, as well as maximum accumulation time (50 ms), and an  $m/z$  range from 300 to 1300 were set. MS/MS scan parameters: Xtreme resolution mode, ICC target at 500,000 with the maximum accumulation time of 100 ms and an isolation width of 2.2  $m/z$  were set. For protein identification, Mascot engine (version 2.4.0, Matrix Science, London, UK) and Database SwissProt (version 2020\_02) were used, and the search parameters were: taxonomy—Homo sapiens (human); enzyme—trypsin; fixed modifications—carbamidomethylation of cysteine (C), variable modification—oxidation of methionine (M); allowed missed cleavages—up to 2; peptide charge +2 and +3; and minimum peptide length—3. For protein assessment, a false discovery rate (FDR) threshold of  $\leq 1\%$  was used, with the minimum of two unique peptides.

#### 4.6. Protein Identification and Label-Free Quantification

Mascot data files (technical duplicates) were loaded into the Proline software (Proline Studio 2.0.1, <http://proline.profiroteomics.fr/>, accessed on 30 March 2022). A minimum score of 20 and an identity  $p$ -value of 0.05 were used to validate PSM (peptide–spectrum matches). A maximum FDR of 1% was used for the protein set. Weighted spectral counts were calculated for each protein according to Abacus [44].

#### 4.7. Pathway Analysis

Gene set enrichment analysis (GSEA) was performed using GSEA v4.2.3 (Broad Institute, Cambridge, MA, USA, <https://www.gsea-msigdb.org/gsea/>, accessed on 16 November 2022). We set the parameters and ran the enrichment tests on the gene set database ([ftp.broadinstitute.org://pub/gsea/gene\\_sets/c2.cp.kegg.v2022.1.Hs.symbols.gmt](ftp.broadinstitute.org://pub/gsea/gene_sets/c2.cp.kegg.v2022.1.Hs.symbols.gmt), accessed on 16 November 2022) for the number of permutations (1000) and the permutation type (phenotype). The data of the signaling pathways from the Kyoto Encyclopedia of Genes and

Genomes (KEGG; [www.genome.jp/kegg](http://www.genome.jp/kegg), accessed on 16 November 2022) were analyzed using the Pathview Web server (<https://pathview.uncc.edu/>, accessed on 16 November 2022).

#### 4.8. Statistical Analysis

Statistical methods (Student's *t*-test or a Wilcoxon test) were used to choose discriminative peaks for the MALDI-TOF/MS data processing. The supervised neural network (SNN), genetic model (GA), and quick classifier (QC) mathematical models for classifying mass spectra were used. The model was built using the 10 peaks of the averaged spectra. The label-free protein quantification analysis between groups (control and CIN3) was used. A beta-binomial test was performed using weighted spectral counts, and a *p*-value computed for each protein set employing the R package BetaBinomial 1.2 was integrated into the Proline Studio software [45]. Using GSEA, the FDR < 0.25 and nominal *p*-value < 0.05 were used to identify significantly enriched pathways.

### 5. Conclusions

The MALDI-TOF/MS results confirmed the differences in protein profiles between the control group and the CIN3 group and can be used as a tool to effectively distinguish between these groups. From the ECM-receptor interaction pathway analysis, it can be concluded that the decrease in the levels of ECM proteins, i.e., HSPG2, COL6A1, COL6A3, SPP1, THBS1, TNC, DAG1, FN1, COMP, GP6, VTN, SDC1, and CD44, may cause disturbances in the interactions of cells with the ECM and play an important role in the development and progression of cervical cancer. However, further research will be required to fully comprehend how proteins impact the dynamic equilibrium of the ECM in related diseases.

**Supplementary Materials:** The following supporting information can be downloaded at: <https://www.mdpi.com/article/10.3390/ijms24032531/s1>.

**Author Contributions:** Conceptualization, P.B.; methodology, P.B. and S.T. (Soňa Tkáčiková); software, P.B. and I.T.; formal analysis, J.S.; resources, P.U. and S.T. (Silvia Toporcerová); data curation, I.T.; writing—original draft preparation, P.B.; writing—review and editing, S.T. (Soňa Tkáčiková) and I.T. All authors have read and agreed to the published version of the manuscript.

**Funding:** This research was funded by the Slovak Research and Development Agency, under project APVV-19-0476, and the Project of the European Regional Development Fund OP Integrated Structure 2014–2020 entitled, under project: ITMS2014+: 313011V446.

**Institutional Review Board Statement:** This study was conducted in accordance with the Declaration of Helsinki and approved by the Ethics Committee of Louis Pasteur University Hospital in Košice (EK/06045/2020).

**Informed Consent Statement:** Informed consent was obtained from all subjects involved in the study.

**Data Availability Statement:** The data presented in this study are available upon request from the corresponding author.

**Conflicts of Interest:** The authors declare no conflict of interest.

### References

1. Bosch, F.X.; Lorincz, A.; Munoz, N.; Meijer, C.J.L.M.; Shah, K.V. The Causal Relation between Human Papillomavirus and Cervical Cancer. *J. Clin. Pathol.* **2002**, *55*, 244–265. [[CrossRef](#)] [[PubMed](#)]
2. Ferlay, J.; Soerjomataram, I.; Dikshit, R.; Eser, S.; Mathers, C.; Rebelo, M.; Parkin, D.M.; Forman, D.; Bray, F. Cancer Incidence and Mortality Worldwide: Sources, Methods and Major Patterns in GLOBOCAN 2012. *Int. J. Cancer* **2014**, *136*, E359–E386. [[CrossRef](#)] [[PubMed](#)]
3. Vergara, N.; Balanda, M.; Hidalgo, W.; Martín, H.S.; Aceituno, A.; Roldán, F.; Villalón, T.; Hott, M.; Espinoza, G.; Quiero, A.; et al. Detection and Genotyping of HPV in Urine Samples from Chilean Women Attending Primary Health Care Centers. *Med. Microbiol. Immunol.* **2017**, *207*, 95–103. [[CrossRef](#)] [[PubMed](#)]
4. Crosbie, E.J.; Einstein, M.H.; Franceschi, S.; Kitchener, H.C. Human Papillomavirus and Cervical Cancer. *Lancet* **2013**, *382*, 889–899. [[CrossRef](#)] [[PubMed](#)]

5. Clifford, G.M.; Smith, J.S.; Aguado, T.; Franceschi, S. Comparison of HPV Type Distribution in High-Grade Cervical Lesions and Cervical Cancer: A Meta-Analysis. *Br. J. Cancer* **2003**, *89*, 101–105. [[CrossRef](#)]
6. de Sanjose, S.; Quint, W.G.V.; Alemany, L.; Geraets, D.T.; Klaustermeier, J.E.; Lloveras, B.; Tous, S.; Felix, A.; Bravo, L.E.; Shin, H.R.; et al. Human Papillomavirus Genotype Attribution in Invasive Cervical Cancer: A Retrospective Cross-Sectional Worldwide Study. *Lancet Oncol.* **2010**, *11*, 1048–1056. [[CrossRef](#)]
7. Greig, J.M.; Ellis, C.J. Biological Agents. In *Occupational Hygiene*; Blackwell Publishing Ltd.: Hoboken, NJ, USA, 2012; pp. 344–359.
8. Herbst, S.; Paladino, A.; de Freitas, S.; Boccardo, E. Alterations in the Expression and Activity of Extracellular Matrix Components in HPV-Associated Infections and Diseases. *Clinics* **2018**, *73*, e551s. [[CrossRef](#)]
9. Elgundi, Z.; Papanicolaou, M.; Major, G.; Cox, T.R.; Melrose, J.; Whitelock, J.M.; Farrugia, B.L. Cancer Metastasis: The Role of the Extracellular Matrix and the Heparan Sulfate Proteoglycan Perlecan. *Front. Oncol.* **2020**, *9*, 1482. [[CrossRef](#)]
10. Sampaio, J.; Ferreira, J.; Santos, A.C.; Bicho, M.; Bicho, M.C. The importance of the extracellular matrix in HPV-associated diseases. In *Cervical Cancer—A Global Public Health Treatise*; Rajkumar, R., Ed.; IntechOpen: London, UK, 2021; pp. 111–130.
11. Senkomago, V.; Des Marais, A.C.; Rahangdale, L.; Vibat, C.R.T.; Erlander, M.G.; Smith, J.S. Comparison of Urine Specimen Collection Times and Testing Fractions for the Detection of High-Risk Human Papillomavirus and High-Grade Cervical Precancer. *J. Clin. Virol.* **2016**, *74*, 26–31. [[CrossRef](#)]
12. Sahasrabudde, V.V.; Gravitt, P.E.; Dunn, S.T.; Robbins, D.; Brown, D.; Allen, R.A.; Eby, Y.J.; Smith, K.M.; Zuna, R.E.; Zhang, R.R.; et al. Evaluation of Clinical Performance of a Novel Urine-Based {HPV} Detection Assay among Women Attending a Colposcopy Clinic. *J. Clin. Virol.* **2014**, *60*, 414–417. [[CrossRef](#)]
13. Pattyn, J.; Van Keer, S.; Téblick, L.; Van Damme, P.; Vorsters, A. HPV DNA Detection in Urine Samples of Women: ‘an Efficacious and Accurate Alternative to Cervical Samples? *Expert Rev. Anti. Infect. Ther.* **2019**, *17*, 755–757. [[CrossRef](#)]
14. Lefeuvre, C.; Pivert, A.; Le Guillou-Guillemette, H.; Lunel-Fabiani, F.; Veillon, P.; Duc-Banaszuk, A.-S.L.; Ducancelle, A. Urinary {HPV} {DNA} Testing as a Tool for Cervical Cancer Screening in Women Who Are Reluctant to Have a Pap Smear in France. *J. Infect.* **2020**, *81*, 248–254. [[CrossRef](#)]
15. Ascitutto, K.C.; Henningson, A.J.; Borgfeldt, H.; Darlin, L.; Borgfeldt, C. Vaginal and urine self-sampling compared to cervical sampling for HPV-testing with the Cobas 4800 HPV test. *Anticancer Res.* **2017**, *37*, 4183–4187. [[CrossRef](#)]
16. Sargent, A.; Fletcher, S.; Bray, K.; Kitchener, H.C.; Crosbie, E.J. Cross-sectional study of HPV testing in self-sampled urine and comparison with matched vaginal and cervical samples in women attending colposcopy for the management of abnormal cervical screening. *BMJ Open* **2019**, *9*, e025388. [[CrossRef](#)]
17. Stanczuk, G.A.; Currie, H.; Baxter, G.; Foster, A.; Gibson, L.; Graham, C.; Cuschieri, K. Cobas 4800 HPV detection in the cervical, vaginal and urine samples of women with high-grade CIN before and after treatment. *J. Clin. Pathol.* **2015**, *68*, 567–570. [[CrossRef](#)]
18. Cho, H.-W.; Ouh, Y.-T.; Hong, J.H.; Min, K.-J.; So, K.A.; Kim, T.J.; Paik, E.S.; Lee, J.; Moon, J.H.; Lee, J.K. Comparison of urine, self-collected vaginal swab, and cervical swab samples for detecting human papillomavirus (HPV) with Roche Cobas HPV, Anyplex II HPV, and RealTime HR-S HPV assay. *J. Virol. Methods* **2019**, *269*, 77–82. [[CrossRef](#)]
19. Van Keer, S.; Tjalma, W.A.A.; Pattyn, J.; Biesmans, S.; Pieters, Z.; Van Ostade, X.; Ieven, M.; Van Damme, P.; Vorsters, A. Human papillomavirus genotype and viral load agreement between paired first-void urine and clinician-collected cervical samples. *Eur. J. Clin. Microbiol. Infect. Dis.* **2018**, *37*, 859–869. [[CrossRef](#)]
20. Bernal, S.; Palomares, J.C.; Artura, A.; Parra, M.; Cabezas, J.L.; Robles, A.; Mazuelos, E.M. Comparison of urine and cervical samples for detecting human papillomavirus (HPV) with the Cobas 4800 HPV test. *J. Clin. Virol.* **2014**, *61*, 548–552. [[CrossRef](#)]
21. Cuzick, J.; Cadman, L.; Ahmad, A.S.; Ho, L.; Terry, G.; Kleeman, M.; Lyons, D.; Austin, J.; Stoler, M.H.; Vibat, C.R.T.; et al. Performance and Diagnostic Accuracy of a Urine-Based Human Papillomavirus Assay in a Referral Population. *Cancer Epidemiol. Biomark. Prev.* **2017**, *26*, 1053–1059. [[CrossRef](#)]
22. Cox, J.; Hein, M.Y.; Lubner, C.A.; Paron, I.; Nagaraj, N.; Mann, M. Accurate Proteome-wide Label-free Quantification by Delayed Normalization and Maximal Peptide Ratio Extraction, Termed MaxLFQ. *Mol. Cell. Proteom.* **2014**, *13*, 2513–2526. [[CrossRef](#)]
23. Wong, J.W.; Cagney, G. An overview of label-free quantitation methods in proteomics by mass spectrometry. *Methods Mol. Biol.* **2010**, *604*, 273–283. [[CrossRef](#)] [[PubMed](#)]
24. Manou, D.; Caon, I.; Bouris, P.; Triantaphyllidou, I.-E.; Giaroni, C.; Passi, A.; Karamanos, N.K.; Vigetti, D.; Theocharis, A.D. The Complex Interplay Between Extracellular Matrix and Cells in Tissues. *Methods Mol. Biol.* **2019**, *1952*, 1–20. [[CrossRef](#)] [[PubMed](#)]
25. Vitale, D.L.; Katakam, S.K.; Greve, B.; Jang, B.; Oh, E.; Alaniz, L.; Götte, M. Proteoglycans and glycosaminoglycans as regulators of cancer stem cell function and therapeutic resistance. *FEBS J.* **2019**, *286*, 2870–2882. [[CrossRef](#)] [[PubMed](#)]
26. Karousou, E.; Misra, S.; Ghatk, S.; Dobra, K.; Götte, M.; Vigetti, D.; Passi, A.; Karamanos, N.K.; Skandalis, S.S. Roles and targeting of the HAS/hyaluronan/CD44 molecular system in cancer. *Matrix Biol.* **2017**, *59*, 3–22. [[CrossRef](#)] [[PubMed](#)]
27. Schaefer, L.; Dikic, I. Autophagy: Instructions from the extracellular matrix. *Matrix Biol.* **2021**, *100–101*, 1–8. [[CrossRef](#)] [[PubMed](#)]
28. van der Flier, A.; Sonnenberg, A. Function and interactions of integrins. *Cell Tissue Res.* **2001**, *305*, 285–298. [[CrossRef](#)]
29. Bao, Y.; Wang, L.; Shi, L.; Yun, F.; Liu, X.; Chen, Y.; Chen, C.; Ren, Y.; Jia, Y. Transcriptome profiling revealed multiple genes and ECM-receptor interaction pathways that may be associated with breast cancer. *Cell. Mol. Biol. Lett.* **2019**, *24*, 38. [[CrossRef](#)]
30. Andersen, M.K.; Rise, K.; Giskeødegård, G.F.; Richardsen, E.; Bertilsson, H.; Størkersen; Bathen, T.F.; Rye, M.; Tessem, M.-B. Integrative metabolic and transcriptomic profiling of prostate cancer tissue containing reactive stroma. *Sci. Rep.* **2018**, *8*, 14269. [[CrossRef](#)]

31. Yan, P.; He, Y.; Xie, K.; Kong, S.; Zhao, W. *In silico* analyses for potential key genes associated with gastric cancer. *PeerJ* **2018**, *6*, e6092. [[CrossRef](#)]
32. Wu, K.; Yi, Y.; Liu, F.; Wu, W.; Chen, Y.; Zhang, W. Identification of key pathways and genes in the progression of cervical cancer using bioinformatics analysis. *Oncol. Lett.* **2018**, *16*, 1003–1009. [[CrossRef](#)]
33. Ramírez-Torres, A.; Gil, J.; Contreras, S.; Ramírez, G.; Valencia-González, H.A.; Salazar-Bustamante, E.; Gómez-Caudillo, L.; García-Carranca, A.; Encarnación-Guevara, S. Quantitative Proteomic Analysis of Cervical Cancer Tissues Identifies Proteins Associated With Cancer Progression. *Cancer Genom. Proteom.* **2022**, *19*, 241–258. [[CrossRef](#)]
34. Giroglou, T.; Florin, L.; Schäfer, F.; Streeck, R.E.; Sapp, M. Human Papillomavirus Infection Requires Cell Surface Heparan Sulfate. *J. Virol.* **2001**, *75*, 1565–1570. [[CrossRef](#)]
35. Buck, C.; Thompson, C.D.; Roberts, J.N.; Müller, M.; Lowy, D.R.; Schiller, J.T. Carrageenan Is a Potent Inhibitor of Papillomavirus Infection. *PLoS Pathog.* **2006**, *2*, e69. [[CrossRef](#)]
36. Winder, S.J. The complexities of dystroglycan. *Trends Biochem. Sci.* **2001**, *26*, 118–124. [[CrossRef](#)]
37. Sgambato, A.; Tarquini, E.; Resci, F.; De Paola, B.; Faraglia, B.; Camerini, A.; Rettino, A.; Migaldi, M.; Cittadini, A.; Zannoni, G.F. Aberrant expression of  $\alpha$ -dystroglycan in cervical and vulvar cancer. *Gynecol. Oncol.* **2006**, *103*, 397–404. [[CrossRef](#)]
38. Zhang, Z.; Zhang, Y.; Ma, Y.; Xiang, S.; Shen, J.; Zhao, Y.; Wu, X.; Li, M.; Yang, X.; Du, F.; et al. Identification of Pathways and Genes Associated with Chemoradiotherapy in Locally Advanced Cervical Cancer. Research Square (preprint), Version 1. *Res. Artic.* **2021**, 1–19. [[CrossRef](#)]
39. Inki, P.; Stenbäck, F.; Grenman, S.; Jalkanen, M. Immunohistochemical localization of syndecan-1 in normal and pathological human uterine cervix. *J. Pathol.* **1994**, *172*, 349–355. [[CrossRef](#)]
40. Shinyo, Y.; Kodama, J.; Hasengaowa; Kusumoto, T.; Hiramatsu, Y. Loss of cell-surface heparan sulfate expression in both cervical intraepithelial neoplasm and invasive cervical cancer. *Gynecol. Oncol.* **2005**, *96*, 776–783. [[CrossRef](#)]
41. Davidson, B.; Goldberg, I.; Gotlieb, W.H.; Ben-Baruch, G.; Kopolovic, J. CD44 expression in uterine cervical intraepithelial neoplasia and squamous cell carcinoma: An immunohistochemical study. *Eur. J. Gynaecol. Oncol.* **1998**, *19*, 46–49.
42. Rey, O.; Lee, S.; Park, N.-H. Human Papillomavirus Type 16 E7 Oncoprotein Represses Transcription of Human Fibronectin. *J. Virol.* **2000**, *74*, 4912–4918. [[CrossRef](#)]
43. Toussaint-Smith, E.; Donner, D.B.; Roman, A. Expression of human papillomavirus type 16 E6 and E7 oncoproteins in primary foreskin keratinocytes is sufficient to alter the expression of angiogenic factors. *Oncogene* **2004**, *23*, 2988–2995. [[CrossRef](#)] [[PubMed](#)]
44. Fermin, D.; Basrur, V.; Yocum, A.K.; Nesvizhskii, A.I. Abacus: A computational tool for extracting and pre-processing spectral count data for label-free quantitative proteomic analysis. *Proteomics* **2011**, *11*, 1340–1345. [[CrossRef](#)] [[PubMed](#)]
45. Pham, T.V.; Piersma, S.R.; Warmoes, M.; Jimenez, C.R. On the beta-binomial model for analysis of spectral count data in label-free tandem mass spectrometry-based proteomics. *Bioinformatics* **2009**, *26*, 363–369. [[CrossRef](#)] [[PubMed](#)]

**Disclaimer/Publisher’s Note:** The statements, opinions and data contained in all publications are solely those of the individual author(s) and contributor(s) and not of MDPI and/or the editor(s). MDPI and/or the editor(s) disclaim responsibility for any injury to people or property resulting from any ideas, methods, instructions or products referred to in the content.